Resonant-phonon terahertz quantum-cascade laser operating at 2.1 THz ($\lambda \simeq 141$ μm)

B.S. Williams, S. Kumar, Q. Hu and J.L. Reno

The development of quantum-cascade lasers (QCLs) at 2.1 THz ($\lambda \simeq 141$ μm), which is the longest wavelength QCL to date without the assistance of magnetic fields, is reported. This laser uses a structure based on resonant-phonon depopulation, and a metal–metal waveguide to obtain high modal confinement with low waveguide losses. Lasing was observed up to a heatsink temperature of 72 K in pulsed mode and 40 K in continuous-wave (CW) mode, and 1.2 mW of power was obtained in CW mode at 17 K.

Introduction: Compact, coherent sources of reasonable power are highly desired in the terahertz frequency range (1–10 THz) for spectroscopy, sensing, and imaging applications, and in particular as local oscillators in heterodyne receiver systems. Solid-state electronic sources of radiation are limited by both transit-time and RC high-frequency roll-offs, and have limited output power (sub-milliwatt) above 1 THz [1]. For this reason, efforts are under way to extend the recently developed terahertz quantum cascade lasers (QCLs) [2–4] to the lowest possible frequencies (longest wavelengths), in order to bridge the gap with electronic sources. However, building QCLs at such long wavelengths becomes increasingly challenging since the intersubband energy separations are extremely small (1 THz corresponds to $\hbar\omega \simeq 4$ meV). It becomes difficult to achieve the selective injection and removal of carriers necessary to obtain an intersubband population inversion, especially as the energy separations become comparable to the subband broadenings. Furthermore, the free-carrier absorption loss scales as λ^2 and thus increases significantly at low frequencies. The first terahertz QCLs were demonstrated at approximately 4.5 THz using chirped superlattice active region structures and semi-insulating (SI) surface plasmon waveguides [2, 3]. Recently, lasers have been reported at ~2.3 THz ($\lambda \sim 130$ μm) in a bound-to-continuum structure, and ~1.9 THz ($\lambda \sim 160$ μm) in an intrawell structure that requires a magnetic field [5]. In this Letter, we report the development of a QCL that operates at a frequency of 2.1 THz ($\lambda \simeq 141$ μm), based on a resonant-phonon active region structure and that uses a low-loss, high-confinement metal–metal waveguide.

Design and fabrication: The resonant-phonon active region design uses a combination of resonant tunnelling and longitudinal-optical (LO) phonon scattering to selectively depopulate the lower radiative state [4]. Lasers based on this structure have recently been demonstrated up to 137 K in pulsed mode at 3.8 THz [6] and up to 93 K in continuous-wave (CW) mode at 3.2 THz [7]. The conduction band diagram for our resonant-phonon design is shown in Fig. 1*a*. The resonant-phonon design concept has a particular advantage for long-wavelength laser operation: the selectivity of the depopulation is determined by the thickness of the 42 Å-thick collector barrier and can be controlled independently from the photon energy. The photon energy (calculated $E_{54} = 9.0$ meV) is determined by the thickness of the 31 Å barrier, which determines the anticrossing gap between $n = 5$ and 4. The small transition energy in this design was obtained using a barrier approximately two monolayers thicker than those in [4, 6, 7]. Since the thickness of the collector barrier determines the 4–3 (and 5–3) anticrossing gap ($\Delta_{43} = 4.3$ meV), by increasing the thickness of the collector barrier level $n = 5$ remains substantially detuned from resonance with $n = 3$ even as E_{54} is reduced. Assuming that the 4–3 resonant tunnelling interaction remains fully coherent, there is no reduction in the depopulation rates of levels 4 and 3 (calculated to be $\tau_4 \simeq \tau_3 \simeq 0.4$ ps due to electron-LO-phonon scattering). Since the upper radiative state $n = 5$ is detuned from resonance with $n = 3$, the upper state wavefunction remains localised and its lifetime remains relatively long (calculated for this structure to be $\tau_{5 \rightarrow (2,1)} \simeq 7$ ps).

The structure, labelled FL173M, was grown in the GaAs/$Al_{0.15}Ga_{0.85}As$ material system by molecular beam epitaxy with 173 cascaded modules. The wafer was processed into low-loss, high-confinement metal–metal waveguide ridge structures by an indium-gold wafer bonding process as described in [7]. The substrate remained unlapped (350 μm thick) and the facets were uncoated. This type of waveguide (shown in Figs. 1*b* and *c*), which is similar in form to a microstrip transmission line, has been demonstrated to be advantageous over conventional SI surface-plasmon terahertz waveguides at higher terahertz frequencies [6, 8], primarily due to its near-unity confinement factor, and its high facet reflectivity. Indeed, the metal–metal waveguide should become even more advantageous at longer wavelengths, as it has no low-frequency cutoff and retains its near-unity confinement. In contrast, the confinement factor of SI-surface-plasmon waveguides drops significantly with decreasing frequency, which often necessitates aggressive thinning of the substrate to prevent mode leakage. Also, since the waveguide height (10 μm) is much smaller than the wavelength, there is a strong impedance mismatch at the waveguide/free-space interface. This high reflectivity minimises facet loss, and thus the threshold current density, although the emitted power is reduced accordingly.

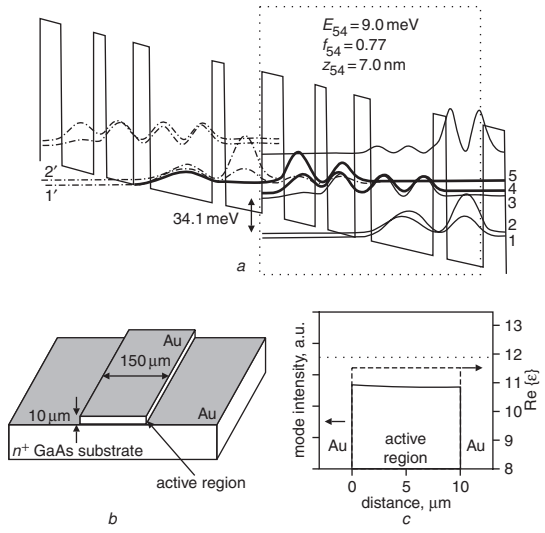

Fig. 1 *Calculated self-consistent conduction band diagram of active region, schematic diagram of metal–metal waveguide, and one-dimensional mode profile and real part of dielectric constant ε(ω) for metal–metal waveguide*

a Calculated self-consistent conduction band diagram of active region
Four-well module outlined by dotted box. Beginning with left injection barrier, layer thicknesses in Å are 56/82/31/70/42/160/34/96. 160 Å well doped at 1.9×10^{16} cm^{-3}
b Schematic of metal–metal waveguide
c One-dimensional mode profile and real part of dielectric constant $\varepsilon(\omega)$ for metal–metal waveguide
——— one-dimensional mode profile
– – – - real part of dielectric constant $\varepsilon(\omega)$

Results: A 150 μm-wide, 1.57 mm-long ridge structure was mounted ridge side up using indium solder on a copper cold stage in a vacuum cryostat. Measured device characteristics are shown in Fig. 2. At 5 K the device displayed a threshold current density of $J_{th} = 562$ A/cm^2 in pulsed mode, and lasing was observed up to a maximum temperature of 72 K. The device lased in continuous-wave (CW) mode up to a heatsink temperature of 40 K, and $J_{th} = 576$ A/cm^2 for a heatsink temperature of 17 K. Lasing took place at frequencies as low as 2.12 THz ($\lambda \simeq 141$ μm) (Fig. 2*b*). This wavelength corresponds to an emitted photon energy of 8.7 meV, which is in good agreement with the calculated value of $E_{54} = 9.0$ meV at design bias. For most of the bias range, the emission is singlemode. The maximum CW power at 17 K was approximately 1.2 mW, measured from a single facet using a thermopile power meter (ScienTech model AC2500).

The maximum operating temperature of this device is limited by the small dynamic current range available beyond threshold. Examination of the voltage against current characteristic (Fig. 2*c*) reveals that the device enters a region of negative differential resistance (NDR) at approximately 10.8 V (1.58 A), as the injector levels become misaligned with the upper state $n = 5$. Beyond this point lasing ceases. An improvement in high-temperature performance should be readily achieved by redesigning the injector to increase the peak current carrying capacity before NDR is reached. Examination of the current against voltage and dV/dI characteristics reveals that a discontinuous drop in differential resistance occurs at threshold. This phenomenon reflects the clamping of the gain and the population inversion at threshold, and can be related to the differences in upper and lower state lifetimes [9]. The fact that such a large discontinuity is observed,

approximately a factor of two, verifies the excellent selectivity of depopulation and injection of this design despite the small subband energy separations. This demonstration of a 2.1 THz QCL confirms that the resonant-phonon design concept is a viable method to achieve lasing at low frequencies, especially in combination with a metal–metal waveguide, which has a nearly wavelength independent high confinement factor.

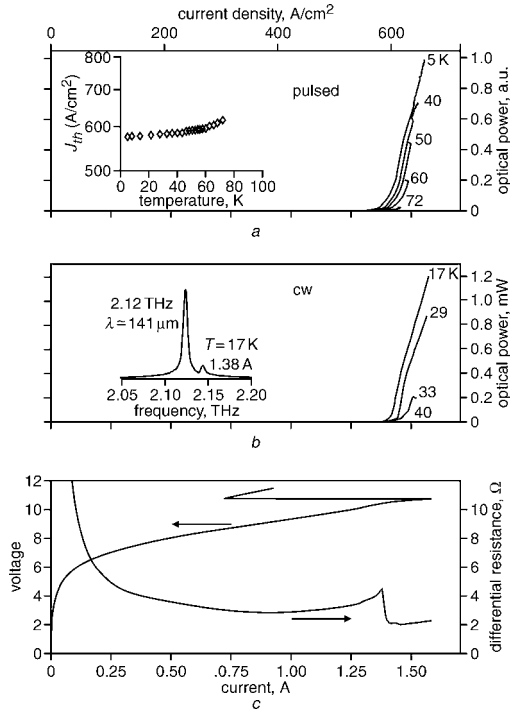

Fig. 2 *Light against current characteristics at various temperatures measured using 200 ns pulses repeated at 1 kHz, and measured in CW mode, and voltage and differential resistance against current measured simultaneously in CW mode*

a Measured using 200 ns pulses repeated at 1 kHz
Inset: Threshold current J_{th} against heatsink temperature
b Measured in CW mode
Inset: CW spectrum taken using Nicolet 850 Fourier transform spectrometer and deuterated triglycine sulfate (DTGS) detector at 0.125 cm^{-1} resolution
c Voltage and differential resistance against current measured simultaneously in CW mode
Due to large power dissipation, heatsink temperature varied from 5 to 17 K over full bias range

Acknowledgments: This work is supported by AFOSR, NASA and NSF. Sandia is a multiprogram laboratory operated by Sandia Corporation, a Lockheed Martin Company, for the US Department of Energy under Contract No. DE-AC04-94AL85000.

4 February 2004
Electronics Letters online no: 20040300
doi: 10.1049/el:20040300

B.S. Williams, S. Kumar and Q. Hu (*Department of Electrical Engineering and Computer Science and Research Laboratory of Electronics, Massachusetts Institute of Technology, Cambridge, Massachusetts 02139, USA*)

J.L. Reno (*Sandia National Laboratories, Department 1123, MS 0601, Albuquerque, New Mexico 87185-0601, USA*)

References

1 Siegel, P.H.: 'Terahertz technology', *IEEE. Trans. Microw. Theory Tech.*, 2002, **50**, pp. 910–928
2 Kohler, R., *et al.*: 'Terahertz semiconductor-heterostructure laser', *Nature*, 2002, **417**, pp. 156–159
3 Rochat, M., *et al.*: 'Low-threshold terahertz quantum-cascade lasers', *Appl. Phys. Lett.*, 2002, **81**, pp. 1381–1383
4 Williams, B.S., *et al.*: '3.4-THz quantum cascade laser based on longitudinal-optical-phonon scattering for depopulation', *Appl. Phys. Lett.*, 2003, **82**, pp. 1015–1017
5 Faist, J.: 2003, Personal communication
6 Williams, B.S., *et al.*: 'Terahertz quantum-cascade laser operating up to 137 K', *Appl. Phys. Lett.*, 2003, **83**, pp. 5142–5144
7 Kumar, S., *et al.*: 'Continuous-wave operation of terahertz quantum-cascade lasers above liquid nitrogen temperature', *Appl. Phys. Lett.*, 2004 (to be published)
8 Williams, B.S., *et al.*: 'Terahertz quantum-cascade laser at $\lambda \simeq 100$ μm using metal waveguide for mode confinement', *Appl. Phys. Lett.*, 2003, **83**, pp. 2124–2126
9 Sirtori, C., *et al.*: 'Resonant tunneling in quantum cascade lasers', *IEEE J. Quantum Electron.*, 1998, **34**, pp. 1722–1729